geoconvention
Calgary • Canada • May 15-17 2023

Physics-informed deep learning to forecast maximum expected magnitude during hydraulic fracturing

Ziyan Li[1], David W. Eaton[1] and Joern Davidsen[2]
[1] Department of Geoscience, University of Calgary
[2] Department of Physics and Astronomy, University of Calgary

Summary

Short-term forecasting of the maximum expected magnitude ($\widehat{M}_{max}$) of induced events during fluid stimulation can be used to minimize the risk of injection-induced seismicity and to improve operational decision-making. Here we propose a physics-based deep learning method to perform probabilistic forecasting of $\widehat{M}_{max}$ during hydraulic fracturing. Our hybrid method combines multi-layer perceptions networks with the Gutenberg-Richter relation, where a slope parameter of *b* =1 is used to represent potential fault activation. We apply this approach to an open-access induced seismicity monitoring dataset from western Canada, which contains more than 18,000 events with a maximum magnitude of 3.2 M_W. Two different models are built based on different data partition methods, where model 1 uses a fixed window method and model 2 uses a cumulative method. The results show that only few induced events exceed the forecasted $\widehat{M}_{max}$ by model 1, possibly from fault reactivation. By contrast, model 2 provides a more conservative probabilistic forecast of $\widehat{M}_{max}$ that bounds all events. Our method could provide a decision-making tool for management of induced seismicity during fluid injection, including hydraulic fracturing and enhanced geothermal systems.

Introduction

Hydraulic fracturing (HF), a fluid stimulation method to enhance permeability by producing fractures in low-permeability reservoir rocks, has the potential to trigger earthquakes by activating existing faults (Bao & Eaton, 2016; Schultz et al., 2020). HF operations typically produce microearthquakes (MEQs) with moment magnitude M_W < 0 (Eaton, 2018; Li et al., 2019). However, induced earthquakes in western Canada, such as the Cardston swarm (Schultz et al., 2015), the Fox Creek area (Schultz et al., 2015), and Fort St. John earthquake sequence (Mahani et al., 2019; Salvage and Eaton, 2022) suggest that HF has the potential to trigger moderate earthquakes with M_W > 4. Such induced events can be large enough to be strongly felt, potentially leading to project suspension and economic loss (Ellsworth, 2013; Keranen et al., 2014; Shipman et al., 2018). Obtaining a probabilistic estimate of the largest expected event magnitude ($\widehat{M}_{max}$) for a given HF operation is useful for hazard assessment (Eaton & Igonin, 2018). Furthermore, accurate short-term operational forecasting of $\widehat{M}_{max}$can inform proactive real-time mitigation strategies for induced seismicity that are required in some monitoring systems (Li et al., 2022; Shipman et al., 2018).

Seismic monitoring data can be analyzed to identify operational MEQs and seismic events triggered by nearby faults (Maxwell et al., 2010; Eyre et al., 2019; Igonin et al., 2021). Operational MEQS during HF typically occur in swarms or clusters that extend away from the wellbore, usually perpendicular to the direction of minimum horizontal stress (Kettlety et al., 2019; Wessels et al.,

2011). In some cases, a reactivated nearby fault can be identified by delayed timing relative to the injection start, and oblique orientation of seismicity clusters with respect to the principal stress directions (Eyre et al., 2019; Igonin et al., 2021; Kettlety et al., 2019; Wessels et al., 2011). Statistically, fault reactivation often results in an increase in seismicity rate accompanied by a decrease in the Gutenberg-Richter b-value (Eaton and Magsouhdi, 2015; Kettlety et al., 2019; Verdon & Budge, 2018).

Li et al. (2022) developed a method for real-time operational forecasting of $\widehat{M}_{max}$ during stimulation. Their method estimates seismic efficiency ratio, an empirically determined fraction of the maximum expected cumulative seismic moment based on injected volume (McGarr, 2014). The seismic efficiency ratio is calibrated during an initial time window of the injection program, and thereafter the forecasted maximum available seismic moment is assumed to be the difference between the projected value and the observed cumulative seismic moment. Although Li et al. (2022) found that their approach provides better estimates than several other approaches, it requires real-time injection data, which is often not available. Hence, we are motivated to seek a method that relies solely on observed seismicity.

Van der Elst et al. (2016) derived an expression for the maximum-likelihood value of $\widehat{M}_{max}$ and its associated probability distribution, assuming that earthquake magnitudes follow the Gutenberg-Richter (G-R) relationship. The parameters required in their formulation are the number of observed events (N_c) above the magnitude of completeness (M_c) and the slope of the semilogarithmic magnitude-frequency distribution (b-value) from the G-R relationship. In this study, we build on this approach and investigate the application of deep learning (DL) techniques to forecast $\widehat{M}_{max}$ as well as the temporal evolution of N_c, which is used to make probabilistic short-term (a few hours) forecasts of $\widehat{M}_{max}$ using the formulation of Van der Elst et al. (2016). For the physics-informed approach, a DL model is applied to forecast Nc, and thus $\widehat{M}_{max}$, based on the assumptions that the magnitude-frequency distribution follows the Gutenberg-Richter relation. We estimate $\widehat{M}_{max}$using a current estimate of *b* is obtained from the seismicity catalogue and an assumed value (*b*=1) based the expectation of this parameter after fault activation (Eaton & Maghsoudi, 2015). The tested methods are based on two different data partition methods, moving window and cumulative, to evaluate the performance of each.

Results and Discussion

We apply our method to the Tony Creek Dual Microseismic Experiment (ToC2ME) dataset, which was acquired by the University of Calgary in 2016 to monitor a four horizontal wells hydraulic fracturing (HF) project (Eaton et al., 2018). The ToC2ME acquisition systems included a 68-station shallow borehole array, six broadband seismometers, and one strong-motion accelerometer. A resulting seismicity catalog obtained using a beamforming method (Igonin, 2021) contains > 18,000 events with well determined magnitudes and hypocenters (Fig. 1), with a maximum magnitude of 3.2 M_W. The ToC2ME dataset contains induced seismicity that occurred during HF treatment of four horizontal wells (A, B, C, and D) that were stimulated over a period of four weeks. Overall, observed seismicity is characterized by $b > 1$, as expected for operational MEQs (Eaton, 2018); however, individual event clusters associated with fault activation show a marked drop in b value (Igonin et al., 2018). Well C was first stimulated from north to south, followed by wells A, B, and D, which were stimulated concurrently using a zipper-fracturing scheme (Eaton, 2018).

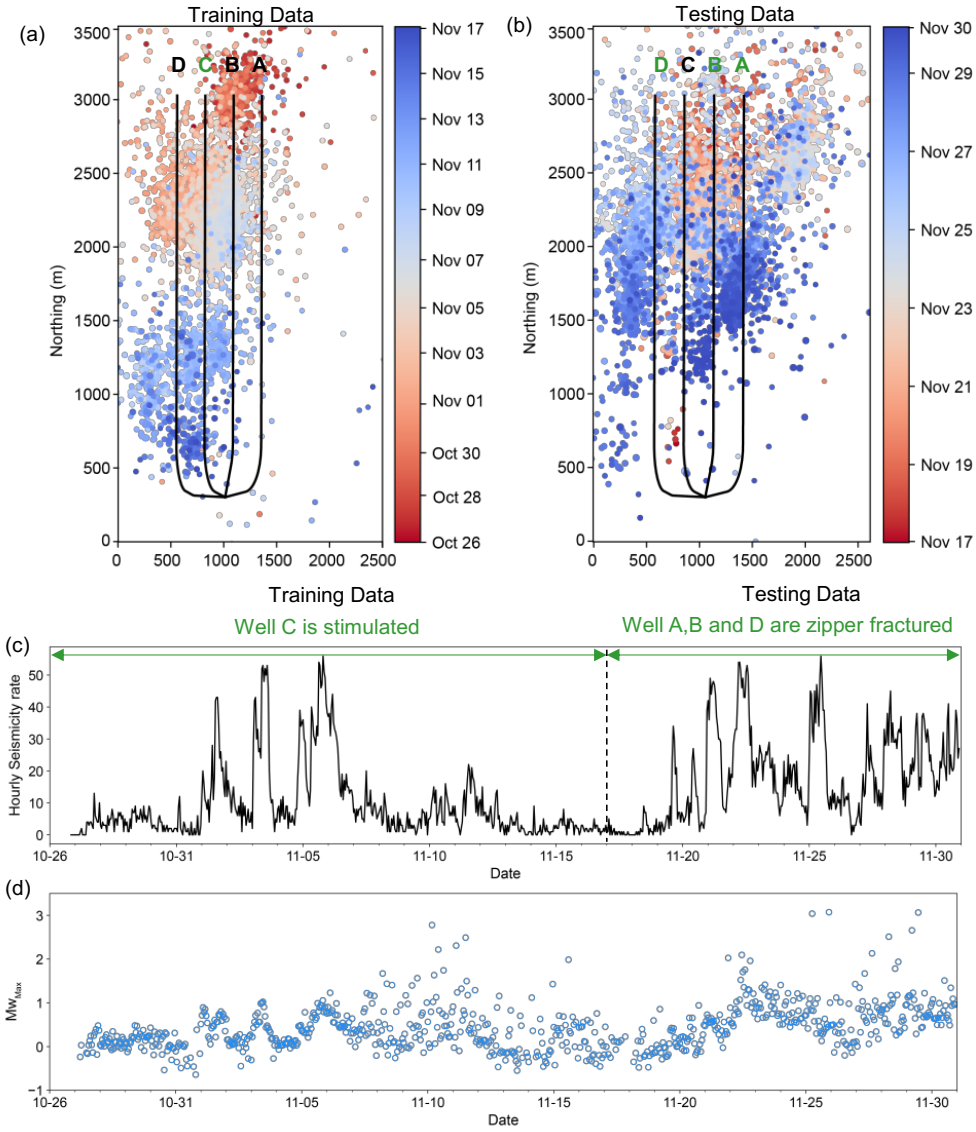

Figure 1. ToC2ME dataset: (a) Seismic event epicenters for the training period, colored by origin time. Four horizontal wells are shown by the black solid lines. (b) As in (a) but for the testing period, where the colored symbols show the microseismicity in the testing dataset. (c) hourly seismicity rate and (d) maximum moment magnitude within moving 1-hour time windows.

We apply both direct DL and physics-informed DL models to forecast $\widehat{M}_{max}$. To explore the impact of data partitioning on the forecasting results, we applied two data partitioning methods to each model. Method 1 is the moving-window method, which employs a window of fixed size (24 hours) to scan the data, with the window advancing by a fixed step size (6 hours). Method 2 is a cumulative method, which increases the window size from its initial size (24 hour) by a specified time period (6 hour) for each step. The DL models use the last four values in the sequence to

predict the subsequent value, based on the corresponding inputs. Specifically, the direct DL model employs the previous four observed M_{max} in the sequence to forecast the next $\widehat{M}_{max}$, using the corresponding inputs. On the other hand, the physics-informed deep learning model considers N_c from the previous four time windows to predict the next $\widehat{N}_c$ in the sequence using the inputs from those windows. Subsequently, $\widehat{M}_{max}$ is estimated based on the statistical method derived by van der Elst et al. (2016).

Figure 2 compares results obtained with the direct DL method and the physics-informed deep learning (PIDL) method. In both graphs, the blue symbols show the maximum magnitude recorded during a 6-hour period. The blue line shows the direct DL forecast for $\widehat{M}_{max}$. The direct DL forecast curves track the observed variations in maximum magnitude reasonably well, based solely on the previous seismicity values, but they exhibit a time lag that limits the practical utility for real-time forecasting. The red curves in Figure 2 show the PIDL forecasts, which are a two-step process wherein DL is used to forecast the seismicity rate, which is then used to forecast the maximum magnitude. The statistical approach developed by van der Elst et al. (2016) enables the probability density function for $\widehat{M}_{max}$ to be computed, allowing confidence limits to be established. In Figure 2, 95% confidence limits are shown using the shaded region.

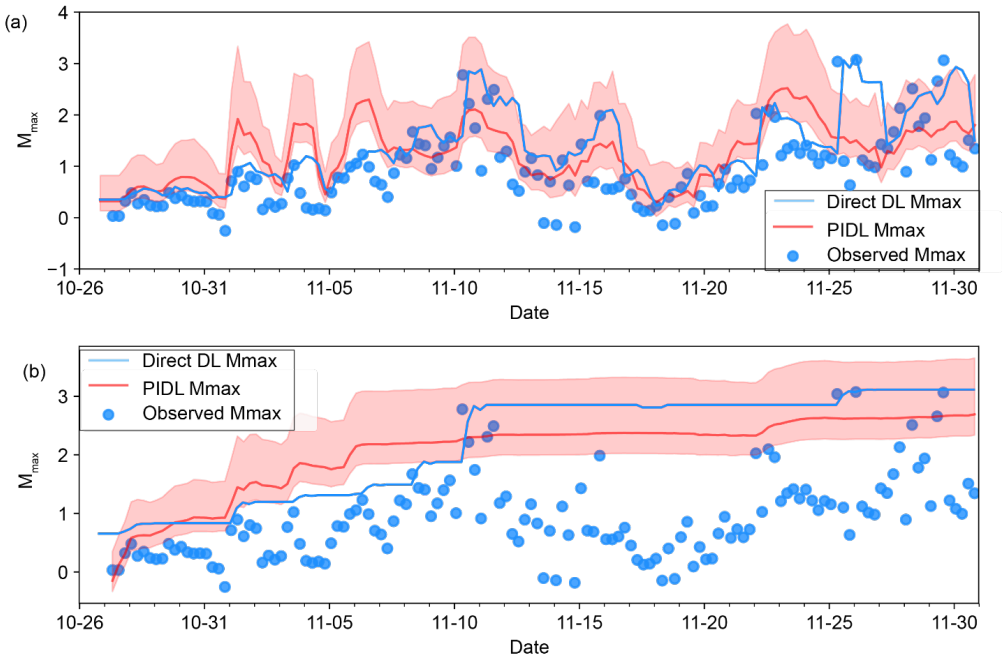

Figure 2. Comparison of direct and physics-informed DL models for forecasting $\widehat{M}_{max}$. (a) Results obtained using data partition method 1. The blue line represents the direct DL model, while the red line shows the results obtained by the physics-informed DL model with current b value. The red shaded area represents the 95% confidence interval. The blue symbols show the actual maximum magnitude of seismic events observed every 6 hours for comparison. (b) Comparison of the direct DL model and the physics-informed DL model for predicting $\widehat{M}_{max}$ using method 2.

The two data partitioning methods that we propose are also compared in Figure 2. In general, the moving-window approach responds to changes in seismicity level, resulting in a floating (up/down) forecast curve. In contrast, the cumulative approach results in monotonically increasing forecast curves for both DL and PIDL methods. The cumulative method thus provides a conservative approach to forecasting $\widehat{M}_{max}$ that does not decline at any point in time, even if the seismicity rate decreases.

Several events on and after 11-25 exceed the PIDL moving window curve (Figure 2a), even considering the 95% confidence limits as indicated by the shaded region. As such, these events represent anomalous magnitude events that fit the criteria for runaway rupture events (Galis et al., 2017; Atkinson et al., 2020). Further work is needed to determine if the occurrence of such events could be incorporated into adaptive traffic light protocols (Mignan et al., 2017).

Conclusions

This study examines the feasibility of forecasting the maximum possibly magnitude of induced seismicity using seismic data solely. We have developed a physics-informed DL model that integrates a DL model with the Gutenberg-Richter relation. This approach is tested using two data partition methods. Method 1 uses a moving window, while method 2 uses a cumulative window that is inherently more conservative, forecasting the largest magnitude of potential induced earthquakes that reactivated by fault. Our results indicate what DL is able to learn from the earthquakes history and will inform earthquake rate forecasting for future events. This result has important implications for industry earthquake forecasting on the field scale.

Acknowledgements

This work was funded by NSERC Alliance Grant ALLRP 548576-2019 entitled “Dynamics of fault activation by hydraulic fracturing: Insights from new technologies”. Sponsors of the Microseismic Industry Consortium are thanked for their ongoing support.

References

Atkinson, G.M., Eaton, D.W. and Igonin, N., 2020. Developments in understanding seismicity triggered by hydraulic fracturing. Nature Reviews Earth & Environment, 1(5), 264-277.

Bao, X., & Eaton, D.W., 2016. Fault activation by hydraulic fracturing in western Canada. Science, 354(6318), 1406-1409.

Eaton, D.W., 2018. Passive seismic monitoring of induced seismicity: Fundamental principles and application to energy technologies. Cambridge University Press.

Eaton, D.W. and Maghsoudi, S., 2015. 2b... or not 2b? Interpreting magnitude distributions from microseismic catalogs. First Break, 33, https://doi.org/10.3997/1365-2397.33.10.83159.

Eaton, D.W. and Igonin, N., 2018. What controls the maximum magnitude of injection-induced earthquakes? The Leading Edge, 37(2), 135-140.

Eaton, D.W., Igonin, N., Poulin, A., Weir, R., Zhang, H., Pellegrino, S. and Rodriguez, G., 2018. Induced seismicity characterization during hydraulic-fracture monitoring with a shallow-wellbore geophone array and broadband sensors. Seismological Research Letters, 89(5), 1641-1651.

Ellsworth, W., 2013. Injection-induced earthquakes. *Science*. 341(6142), 1225942.

Eyre, T.S., Eaton, D.W., Zecevic, M., D'Amico, D. and Kolos, D., 2019. Microseismicity reveals fault activation before Mw 4.1 hydraulic-fracturing induced earthquake. Geophysical Journal International, 218(1), 534-546.

Galis, M., Ampuero, J.P., Mai, P.M. and Cappa, F., 2017. Induced seismicity provides insight into why earthquake ruptures stop. Science Advances, 3(12), eaap7528.

Igonin, N., 2021. Hydraulic-fracturing induced seismicity in Alberta, Canada: Analysis and interpretation using dense local arrays. PhD thesis, The University of Calgary. http://dx.doi.org/10.11575/PRISM/38820

Igonin, N., Zecevic, M. and Eaton, D.W., 2018. Bilinear magnitude-frequency distributions and characteristic earthquakes during hydraulic fracturing. Geophysical Research Letters, 45(23), https://doi.org/10.1029/2018GL079746

Igonin, N., Verdon, J.P., Kendall, J.M. and Eaton, D.W., 2021. Large-scale fracture systems are permeable pathways for fault activation during hydraulic fracturing. Journal of Geophysical Research: Solid Earth, 126(3), p.e2020JB020311.

Keranen, K.M., Weingarten, M., Abers, G.A., Bekins, B.A. and Ge, S., 2014. Sharp increase in central Oklahoma seismicity since 2008 induced by massive wastewater injection. Science, 345(6195), 448-451.

Kettlety, T., Verdon, J.P., Werner, M.J., Kendall, J.M. and Budge, J., 2019. Investigating the role of elastostatic stress transfer during hydraulic fracturing-induced fault activation. Geophysical Journal International, 217(2), 1200-1216.

Li, L., Tan, J., Wood, D.A., Zhao, Z., Becker, D., Lyu, Q., Shu, B. and Chen, H., 2019. A review of the current status of induced seismicity monitoring for hydraulic fracturing in unconventional tight oil and gas reservoirs. Fuel, 242, 195-210.

Li, Z., Eaton, D. and Davidsen, J., 2022. Short-term forecasting of Mmax during hydraulic fracturing. Scientific Reports, 12(1), 1-12.

Mahani, A. B., Kao, H., Atkinson, G. M., Assatourians, K., Addo, K., & Liu, Y. (2019). Ground-motion characteristics of the 30 November 2018 injection-induced earthquake sequence in Northeast British Columbia, Canada. Seismological Research Letters, 90(4), 1457-1467.

Maxwell, S.C., Rutledge, J., Jones, R. and Fehler, M., 2010. Petroleum reservoir characterization using downhole microseismic monitoring. Geophysics, 75(5), 75A129-75A137.

McGarr, A., 2014. Maximum magnitude earthquakes induced by fluid injection. Journal of Geophysical Research: Solid Earth, 119(2), 1008-1019.

Mignan, A., Broccardo, M., Wiemer, S. and Giardini, D., 2017. Induced seismicity closed-form traffic light system for actuarial decision-making during deep fluid injections. Scientific Reports, 7(1), https://doi.org/10.1038/s41598-017-13585-9.

Salvage, R. O., & Eaton, D. W. (2022). The Influence of a Transitional Stress Regime on the Source Characteristics of Induced Seismicity and Fault Activation: Evidence from the 30 November 2018 Fort St. John M_L 4.5 Induced Earthquake Sequence. Bulletin of the Seismological Society of America, 112(3), 1336-1355.

Schultz, R., Mei, S., Pană, D., Stern, V., Gu, Y.J., Kim, A. and Eaton, D., 2015. The Cardston Earthquake Swarm and Hydraulic Fracturing of the Exshaw Formation (Alberta Bakken Play). Bulletin of the Seismological Society of America, 105(6), 2871-2884.

Schultz, R., Skoumal, R.J., Brudzinski, M.R., Eaton, D.W., Baptie, B. and Ellsworth, W., 2020. Hydraulic fracturing-induced seismicity. Reviews of Geophysics, 58(3), e2019RG000695.

Shipman, T., MacDonald, R. and Byrnes, T., 2018. Experiences and learnings from induced seismicity regulation in Alberta. Interpretation, 6(2), pp.SE15-SE21.Shipman, T., MacDonald, R., & Byrnes, T. (2018). Experiences and learnings from induced seismicity regulation in Alberta. Interpretation, 6(2), SE15-SE21.

Van der Elst, N.J., Page, M.T., Weiser, D.A., Goebel, T.H. and Hosseini, S.M., 2016. Induced earthquake magnitudes are as large as (statistically) expected. Journal of Geophysical Research: Solid Earth, 121(6), 4575-4590.

Verdon, J.P. and Budge, J., 2018. Examining the capability of statistical models to mitigate induced seismicity during hydraulic fracturing of shale gas reservoirs. Bulletin of the Seismological Society of America, 108(2), 690-701.

Wessels, S.A., De La Peña, A., Kratz, M., Williams-Stroud, S. and Jbeili, T., 2011. Identifying faults and fractures in unconventional reservoirs through microseismic monitoring. First break, 29(7).